

Off-stoichiometric softening and polytypic transformations in the plastic deformation of the C14 Fe₂Nb Laves phase

A.N. Ladines,¹ R. Drautz,¹ and T. Hammerschmidt¹

¹*Atomistic Modelling and Simulation, ICAMS, Ruhr-Universität Bochum, D-44801 Bochum, Germany*

Plastic deformation of the brittle C14-Fe₂Nb Laves phase occurs mostly by basal slip due to the complex crystal structure. Here, we compare the barriers for basal slip for the known mechanisms of direct slip, synchroshear and undulating slip using density functional theory calculations. According to our calculated generalized stacking fault (SF) energies, the most favorable mechanisms are synchroshear and undulating slip. Both mechanisms lead to stable SF with a formation energy of 50 mJ/m² through the same unstable SF configuration at the transition. The energy barrier of approximately 3 J/m² indicates a low dislocation mobility as expected from the brittle character. We also determine the influence of vacancies and antisite defects on the formation energy of stable and unstable SF. Both kinds of point defects tend to lower the energy barrier on both sides of 2:1 stoichiometry. This explains the experimentally observed off-stoichiometric softening of C14-Fe₂Nb. The small energy differences between the Fe₂Nb Laves phase polytypes raises the question if there are further deformation mechanisms with low barrier. Therefore, we additionally consider transformations between C14, C15 and C36 Laves phases as further deformation mechanism. Our calculations for polytypic transformations by successive synchroshear steps show that the corresponding energy barriers are in fact very similar to the energy barrier for basal slip in C14. This suggests that the energy needed to create a stable SF in C14 by synchroshear is also sufficient to initiate polytypic transformations where existing SFs in C14 are further transformed to form C15 or C36 Laves phases.

I. INTRODUCTION

One of the most commonly observed group of crystal structures are the topologically close-packed (TCP) phases¹ and particularly the Laves phases C14, C15, C36. Laves phases have been subject to extensive theoretical and experimental studies, see e.g. Ref. 2 for a recent review. Their structural stability is to a large degree governed by differences in atomic size and the average number of valence electrons³⁻⁶. The Laves phases are inherently brittle at low temperatures (< 0.6T_m)⁷, a result of the complex crystal structure of the Laves phases that lacks straightforward slip mechanisms^{8,9}.

The crystal structure of the Laves phases comprises two-third polyhedra with coordination number Z=12 and one-third Z=16 polyhedra, occupied preferably by small (S) and large (L) atoms, respectively. It consists of a close-packed stacking of atomic layers of the 6 · 3 · 6 · 3-type in the Schäfli notation known as Kagomé layer and a puckered triple layer of L-S-L atoms along the ⟨0001⟩ direction in the hexagonal (h) representation (see Fig. 1(a)) or along the ⟨111⟩ direction in the cubic (c) representation. The interlayer spacing within the puckered layer is approximately one third of that between the triple layer and the Kagomé layer. The atomic layers can be centered on either of the three high-symmetry points which are related by the Shockley Burgers vectors $b_1 = a/3\langle 1\bar{1}00 \rangle$ -h or $b_2 = a/6\langle 112 \rangle$ -c as shown in Fig. 1(b). In the C14-Fe₂Nb Laves phase, the Fe atoms correspond to S atoms on 2a and 6h sites with Z=12 and the Nb atoms correspond to L atoms on 4f sites with Z=16.

The stacking sequence needs to fulfill certain requirements in order to achieve close packing: the lower part of the triple layer occupies the center of the Kagomé layer

while the middle sublayer occupies one of the two other high symmetry points. This results in two variants of the triple layer, t and its reflection t' . The top layer is centered on the remaining high symmetry point. Depending on the centering of the Kagomé layer, the quadruple layer can be of type X , Y , Z or their reflections X' , Y' , Z' . The X quadruple layer, e.g., corresponds to an $Aac\beta$ stacking sequence. (Small atoms on the A, B and C points are denoted as a, b, and c while large atoms on these sites are referred to as α , β and γ .) The various stacking sequences of quadruple layers give rise to the Laves phase polytypes C14, C15 and C36 (see Ref. 10 for a detailed discussion) with the three shortest repeating periods XY' (h), XYZ (c) and $XY'X'Y$ (h).

The experimentally observable slip in Laves phases occurs mostly in the basal plane¹¹⁻¹³. The three known basal deformation mechanisms for Laves phases are direct slip, synchroshear¹⁴ and undulating slip¹⁵. Their relative importance is determined by the generalized stacking fault energy (SFE) curve^{16,17}. While hardly accessible by experiment, the generalized SFE can be determined by atomistic calculations using electronic-structure methods¹⁸. For several Laves phase compounds, the generalized SFE has been determined by density-functional theory (DFT) calculations¹⁹⁻²¹. For the technologically important C14-Fe₂Nb Laves phase²², however, atomistic insight to the governing mechanism of plastic deformation is still missing.

In this study, we perform DFT calculations to determine the generalized SFE curves in the C14-Fe₂Nb Laves phase. We compare the deformation by direct slip, synchroshear and undulating slip in defect-free, stoichiometric C14-Fe₂Nb, followed by an analysis of the influence of off-stoichiometric compositions due to vacancy or antisite

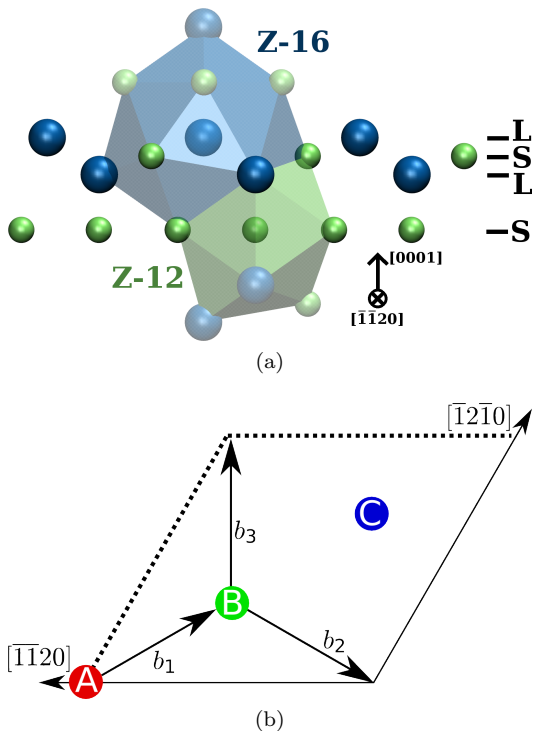


FIG. 1: (a) Stacking sequence of the elementary quadruple layer in Laves phases viewed parallel to the basal plane. The Kagomé layer contains smaller atom only while the triple layer is a stacking of large-small-large atoms. (b) High symmetry points and Burgers vectors in the hexagonal lattice representation of Laves phases.

defects. In addition we assess the possibility of polytypic transformations from C14 to C15 and C36 by successive transformation via intermediate SF configurations.

II. METHODOLOGY

The DFT calculations presented in this work were performed with the VASP software (version 5.4)^{23–25} using the projector-augmented wave method²⁶. The generalized gradient approximation to the exchange-correlation functional²⁷ and pseudo-potentials with p semicore states were employed. A planewave cut-off energy of 450 eV and a k -point spacing of 6 \AA^{-1} was required to converge the total energies to less than 1 meV/atom. A supercell consisting of 24 atomic layers (36 atoms) was used in the calculation of the bulk SFE. The initial magnetic configuration was set to the energetically most favorable arrangement for the Fe_2Nb C14 Laves phase, i.e. (UD)/(UD)/U on the $2a/6h/4f$ sites, as determined previously⁶. No constraints on the spins were applied during the electronic self-consistency. The reference structure was obtained by optimizing the lattice parameters and the atomic positions of the bulk C14- Fe_2Nb Laves phase. For the deformation along the generalized SFE curve we use sheared periodic boundary conditions that vary as a

function of the deformation parameter¹⁹. During the deformation, the ionic positions were allowed to relax while the deformed simulation cell was kept fixed. For the simulations with vacancy and antisite defects, a $2 \times 2 \times 2$ supercell (96 atoms) was used to avoid interaction of the points defects with their periodic boundary image.

III. RESULTS AND DISCUSSION

A. Basal deformation of stoichiometric C14- Fe_2Nb

1. Deformation mechanisms

There are at least three basal deformation modes in Laves phases, shown schematically in Fig. 2: (i) The most apparent mechanism is direct slip between the Kagomé and the triple layer with Burgers vector $a/3 \langle 10\bar{1}0 \rangle$ -h. (ii) The synchroshear slip mechanism involves a synchronous displacement of the middle and top layer by $a/3 \langle 10\bar{1}0 \rangle$ -h and $a/3 \langle 01\bar{1}0 \rangle$ -h, respectively¹⁴. (iii) The undulating slip mechanism is a deformation process which involves crystallographic slip and atomic shuffling. This slip mechanism was shown to have a lower energy barrier in the Cr_2Nb system compared to the previously discussed deformation modes¹⁵.

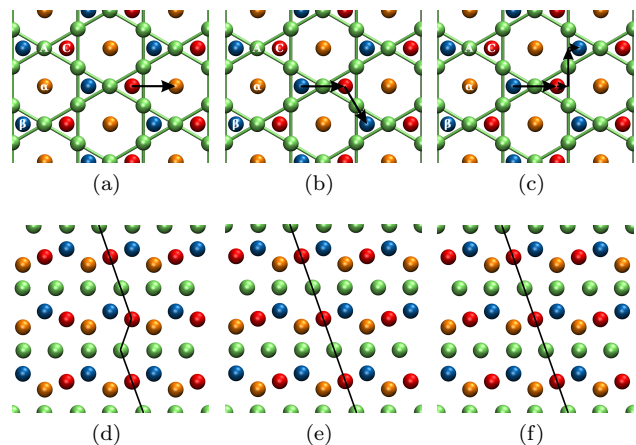


FIG. 2: Basal deformation modes in Laves phase: direct slip (left), synchroshear (middle) and undulating slip (right) viewed along $[0001]$ (Figs. a-c) and $[\bar{1}\bar{1}20]$ (d-f). The arrows in the upper figures indicate the motion in the quadruple layer. The upper half of the crystal above the deformation plane is also shifted in the slip direction by one Burgers vector. The solid lines in the lower figures indicate the layer sequence in the resulting SF.

2. Generalized SFE curves for C14- Fe_2Nb

Experimental analysis of deformed Fe_2Nb samples identified SF structures as remainders of basal slip deformation^{28,29} and suggested synchroshear as dominant

deformation process. However, undulating slip cannot be excluded as the resulting local C15 stacking sequence is the same for synchroshear and undulating slip (see Fig. 2). Here, we determine the most favorable basal deformation mechanism in C14-Fe₂Nb by DFT calculations of the energy barrier along the generalized SFE curves shown in Fig. 3.

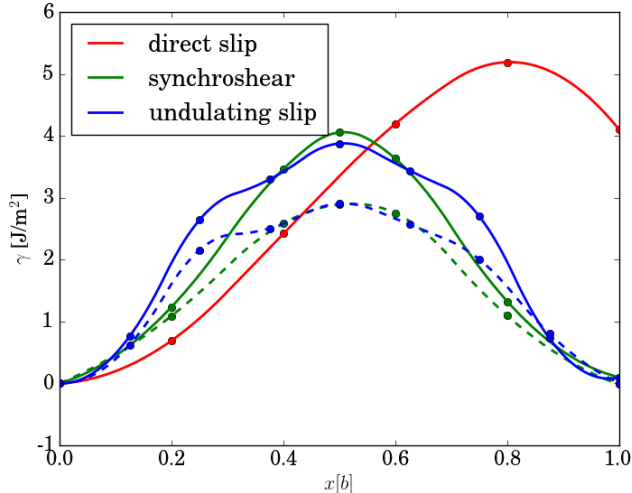


FIG. 3: Generalized SFE curve corresponding to the basal deformation modes in C14-Fe₂Nb. The points denote the calculated SFE while the lines are second-order spline interpolations. The dashed lines connect the stacking fault energies in the relaxed configuration.

Direct slip involves rather small energies in the initial stage due to the large free volume between the Kagomé layer and the triple layer which then increase as the Fe atoms in the Kagomé layer approach the Nb atoms in the adjacent layer. The energy barrier for direct slip, given by the maximum of the generalized SFE curve, is the largest among the three deformation mechanisms. This deformation results in a metastable configuration which may further develop to a stable configuration through a similar slip along the two other Burgers vectors. Synchroshear and undulating slip, in contrast, lead to a stable SF with a formation energy of ≈ 50 mJ/m². The energy barrier to arrive at this stable SF is reported in Fig. 3 for both, relaxed and unrelaxed configurations. For the unrelaxed configurations, the undulating slip has the lowest energy barrier of the three deformation modes. Upon relaxation, the synchroshear and undulating slip lead to the same unstable SF configuration at the maximum of the generalized SFE curve and hence exhibit the same energy barrier of approximately 3 J/m². This finding is in line with the experimentally observed SF configuration after deformation^{28,29}. Similar results were obtained recently with a classical potential for the case of C14-Mg₂Ca³⁰.

Overall, the rather large barriers indicate that plastic deformation of the C14-Fe₂Nb Laves phase by dislocation nucleation in the basal plane is associated with large stresses. This raises the questions (i) if the barriers can

be reduced, e.g., by changing the chemical composition (see Sec. III B), (ii) if further processes are activated by the required large stresses (see Sec. III C) and (iii) if the experimentally observed SF in C14-Fe₂Nb could be remains of other, not yet identified processes.

B. Off-stoichiometric softening

1. Formation energy of point defects in C14-Fe₂Nb

Many Laves phases are known to form also at off-stoichiometric compositions³¹. The deviation from the 2:1 composition is attributed to vacancies or antisite atoms, primarily of the smaller atom. These point defects are known to have profound impact on the mechanical properties³². The vacancy formation-energy

$$E_f^{\text{vacancy}} = \frac{(1 - x_D)\Delta H_{\text{vacancy}} - \Delta H_{\text{ideal}}}{x_D} \quad (1)$$

and the antisite formation energy

$$E_f^{\text{antisite}} = \frac{\Delta H_{\text{antisite}} - \Delta H_{\text{ideal}}}{x_D} \quad (2)$$

are computed from the difference in the heat of formation obtained by DFT as outlined in the Appendix. x_D is the fraction of defects to the number of atoms in the supercell. The heat of formation of the supercells with and without defect are computed with respect to the bcc ground-states of Fe and Nb. (A previously reported simpler accounting for changes in chemical composition due to defect formation leads to qualitatively comparable results³³.)

TABLE I: Vacancy and antisite formation-energies in C14-Fe₂Nb.

site	$E_f^{\text{vac}}(\text{eV})$	$E_f^{\text{antisite}}(\text{eV})$
2a (Fe)	2.71	0.60
6h (Fe)	2.57	0.87
4f (Nb)	2.77	1.33

Our DFT calculations, compiled in Tab. I, show that the formation energies of the different antisite defects are considerably lower than all vacancy formation energies. We therefore expect that antisite defects are the dominant intrinsic defects in Fe₂Nb. This is consistent with the experimentally observed absence of vacancies in C14-Fe₂Nb³⁴.

The energetic ordering of the antisite defects in Tab. I is related to the size of the Fe/Nb atoms on one hand and the Z12/Z16 coordination polyhedra on the other hand: The DFT results indicate that it is energetically favorable by about at least 0.5 eV to squeeze a comparably larger Nb atom in an empty Z12 polyhedron of a removed Fe atom than to fill an empty Z16 polyhedron of a removed Nb atom with a comparably smaller Fe atom.

2. Influence of point defects on generalized SFE

An early work on C14-Fe₂Nb reported that the antisite defects cause a hardening on both sides of the 2:1 stoichiometry³⁴. More recent works made contrasting observations of progressive softening for off-stoichiometric compositions^{35,36}. This softening was suggested to arise from the free volume generated by the vacancy or antisite which facilitates the motion of synchro-Shockley dislocations^{10,37}. In order to shed light on these contrasting findings, we compute the influence of vacancy and antisite defects on the barrier for plastic deformation in C14-Fe₂Nb. In particular, we compute the formation energy of the unstable and stable SF ($x = 0.5$ and $x = 1.0$ in Fig. 3) with either of these two point defects present in different distances from the SF plane.

Our calculations, compiled in Fig. 4, show that nearly all defects increase the formation energy of the stable stacking fault (γ^{stable}) and decrease the energy barrier for synchroshear ($\gamma^{unstable} - \gamma^{stable}$). The only exception with a notably increased barrier is the antisite defect on 2a Fe sites in 7.5Å distance from the SF plane. The origin of this exception is the convergence to a magnetic state that is different from the one of the unsheared structure. The variation of the SF energy with distance for the individual defects shows that only vacancies on 2a Fe sites are weakly attracted to the SF plane while all other vacancy and antisite defects are weakly repelled. From the overall rather small thermodynamic driving forces for segregation we expect that the local site occupation is not considerably affected by the presence of the stable SF.

In summary, our calculations show that deviations from the 2:1 composition due to vacancies or due to antisite defects lead to a softening of C14-Fe₂Nb on both sides of the stoichiometry due to a reduced energy barrier for shearing. This finding explains the recent experimental observations^{35,36} of softening for off-stoichiometric compositions.

C. Polytypic transformations

The stresses that are needed to overcome the computed barriers for basal slip (Sec. III A) are so large that one might expect that other processes are initiated, too. A particularly likely candidate are stress-induced transformations that are known from other Laves phase compounds³⁸. Here, we compute the energy barriers of polytypic transformation between C14, C15 and C36 Laves phases by successive synchroshear, see Fig. 5.

A synchroshear deformation can be seen as propagation of two Shockley dislocations through the quadruple layer which leads to a macroscopic shear strain. The Burgers vector of the Shockley dislocations can be one of those shown in Fig. 1(b). If the layer of small atoms in the triple layer moves along $-b_1$, the upper layer of large atoms must move in synch either along b_2 or b_3 . This deformation transforms a quadruple layer t to t' or vice

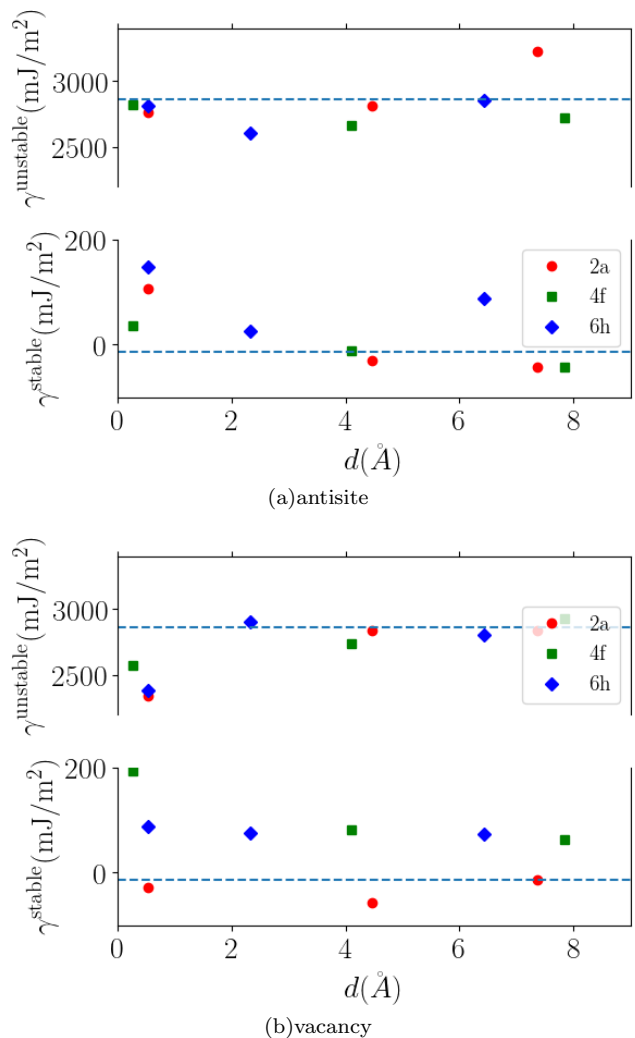


FIG. 4: Influence of (a) antisite defect and (b) vacancy on the energy of stable and unstable stacking fault in C14-Fe₂Nb as a function of the distance from the respective stacking fault plane.

versa. Applying an equal number of these three equivalent Burgers vectors can lead to an alternative polytypic transformation without macroscopic strain¹⁰. A transformation between Laves phase polytypes can also be realized if the number of $t \rightarrow t'$ and $t' \rightarrow t$ synchroshear steps are equal. This is the case for the C14→C36 transformation shown in Fig.5(b). Therefore, it is possible to transform the C14 structure to the C15 structure in two ways¹⁹ by a series of synchroshear steps as illustrated in Fig. 5. In the plastic deformation of C14-Fe₂Nb, an already formed stable SF could transform further by successive synchroshear steps that eventually lead to a precipitate of C15 or C36.

We compare the formation of a new stable SF to a further synchroshear of an existing SF, in terms of the energy profile along the polytypic transformation by successive synchroshear. We used unrelaxed atomic structures along the transformation path that we compare to

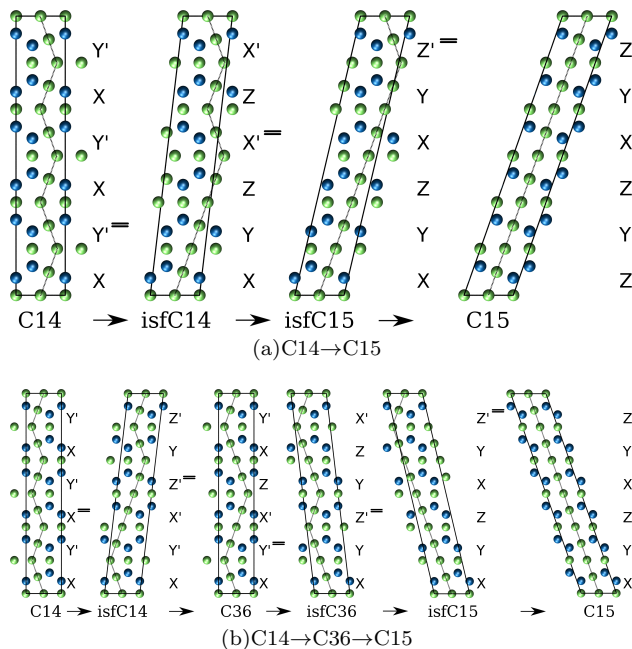


FIG. 5: Series of synchroshear deformations of the polytypic transformations routes from C14 to C15 with intermediate intrinsic stacking fault (isf) configurations. The synchroshear plane and the characteristic layer configuration are indicated.

the unrelaxed structures of the generalized SFE for basal slip in Fig. 3. From our calculations for the SFE we expect that including the structural relaxation would lead to an overall scaling that would not alter our conclusions.

In Fig. 6 we plot the computed change in energy with respect to the initial C14-Fe₂Nb for the corresponding configurations. The first insight from our DFT results is that all intermediate stable states of the polytypic transformation, i.e. the Laves phases as well as their intrinsic stacking faults, are very close in energy within a range of less than 20 meV per atom. The formation energy of the SF in C36 is negative since C36 is predicted to be more energetically favorable in our spin-polarized DFT calculations. The correct prediction of the C14 ground state requires to extend the DFT calculations to a proper treatment of paramagnetism³⁹ which would then be too computationally involved for the large supercells required for this work. The second insight is that the energy barriers between the intermediate stable states of the synchroshear series are almost identical (≈ 140 meV/at = 4 J/m²). Moreover, they are very similar to the energy barrier for a single synchroshear or undulating slip in the generalized SFE curve of C14-Fe₂Nb for unrelaxed atomic positions (Fig.3). This indicates that pressures which lead to the formation of an intrinsic SF in C14-Fe₂Nb may also initiate a polytypic transformation of C14 to C15 or C36 by further transforming already existing SFs.

The energy profile along the polytypic transformation by a series of synchroshear steps can be rationalized in

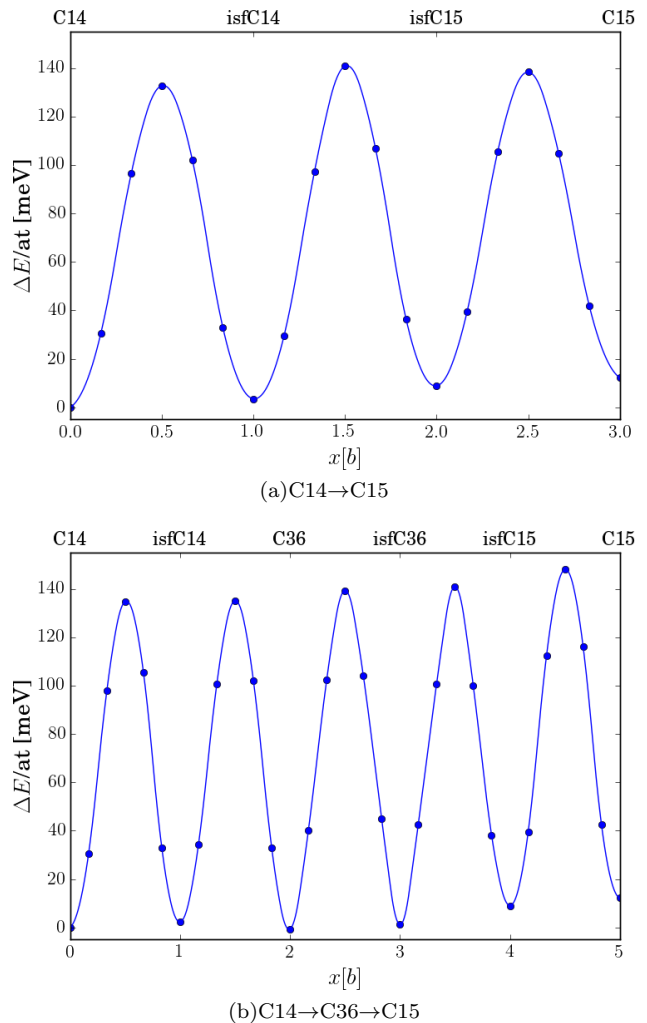


FIG. 6: Change in energy along polytypic transformations from C14 to C15 and C36. The points denote the DFT calculations; the lines are interpolations to guide the eye.

terms of the corresponding deformation of the Z12 and Z16 Frank Kasper polyhedra. A measure of this deformation is the change in the nearest-neighbour bond-lengths, σ , of the S and L atoms in the synchrosheared quadruple layer shown in Fig. 7. The change in bond lengths along the synchroshear steps is similar for the S and L atoms in the quadruple layer and reaches values of nearly 0.5 Å. This considerable change is directly related to the energy increase at the transition point of the energy profile in Fig. 6.

IV. CONCLUSIONS

We perform DFT calculations on the role of different basal slip mechanisms for the plastic deformations of the C14-Fe₂Nb Laves phase. The generalized stacking-fault energy curves show that synchroshear and undulating slip pass the same transition state with an energy barrier of

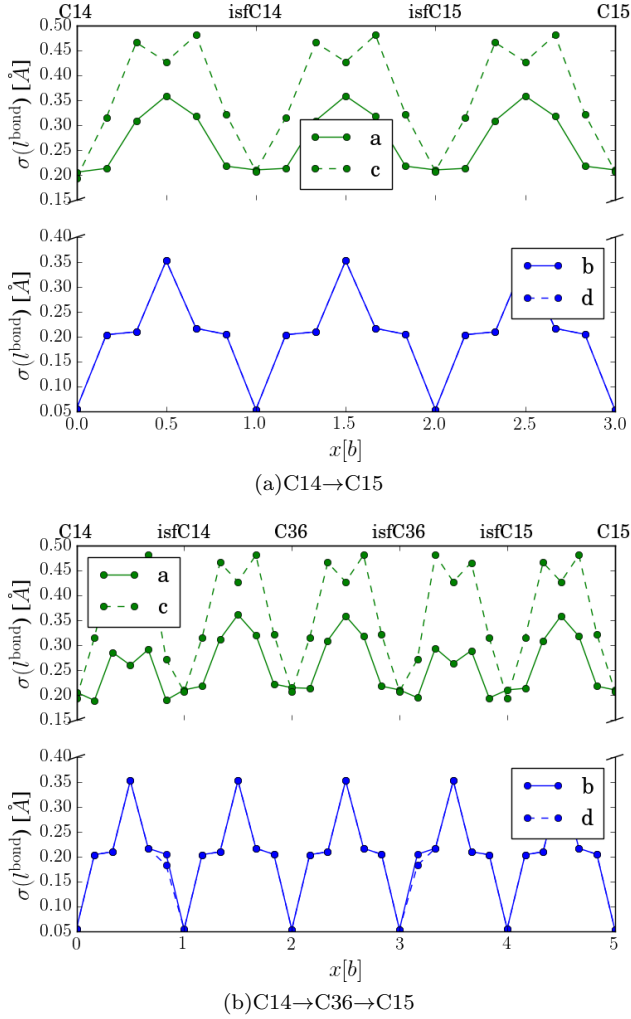


FIG. 7: Bond lengths in the coordination polyhedra of atoms comprising the synchrosheared quadruple layer along the transformation path: (a) C14→C15 (b) C14→C36→C15. The labels a, b, c and d correspond to the atoms in the stacking sequence S-L-S-L in Fig. 1(a).

3 J/m^2 that is considerably lower than direct slip. The experimentally observed stacking fault configurations are in line with the final structures of both, synchroshear and undulating slip. However, the large energy barriers for the considered mechanisms and the rather low formation energy of stable SF in C14 may indicate the existence of not yet considered mechanisms that lead to the experimentally observed SF configurations.

Our DFT calculations for the stable and unstable SF in the presence of vacancies and antisite defects show that the barrier for synchroshear is decreased. This finding explains the experimentally observed softening of C14-Fe₂Nb by off-stoichiometric compositions on both sides of the 2:1 composition.

In order to assess the possibility of polytypic transformations, we compute the energy profile of the transformation from C15 to C14 and C36 by a series of synchros-

hear deformations. The energy barriers are very similar for the different steps of the deformation series and moreover very similar to synchroshear and undulating slip. This indicates that the pressures which lead to plastic deformation of C14-Fe₂Nb by stacking fault formation can also initiate polytypic transformation of C14 to C15 or C36 through successive synchroshear of existing SF.

Appendix: Formation energy of point defects

For the energetic ranking of the different point defects in C14-Fe₂Nb, we compute the formation energy per atom of a general structure with N Fe atoms and M Nb atoms as

$$\Delta H_{\text{struc}}^{N,M} = \frac{E_{\text{struc}}^{N,M} - NE_{\text{Fe}} - ME_{\text{Nb}}}{N + M} \quad (3)$$

where $E_{\text{struc}}^{N,M}$, E_{Fe} and E_{Nb} are the DFT total energies of the respective general structure and the energetically most favorable bcc structure of Fe and Nb. This choice corresponds to the chemical potential of the DFT convex hull at T=0K. The superscripts denote the number of Fe and Nb atoms in the DFT simulation cell. The bcc simulation cells are assumed to contain one atom. The formation energy per atom of ideal C14-Fe₂Nb without defects is given by

$$\Delta H_{\text{C14}}^{N,M} = \frac{E_{\text{C14}}^{N,M} - NE_{\text{Fe}} - ME_{\text{Nb}}}{N + M} \quad (4)$$

and referred to as ΔH_{ideal} in Eqs. 1 and 2. The formation of vacancies and antisite defects in C14-Fe₂Nb alters the chemical composition. In order to compute the defect formation energy, we need the energy difference between ideal bulk and the defect structure plus additional terms that balance the total number of atoms for each species.

For vacancies, the formation energy per atom of a supercell structure with a missing Fe atom ('C14vacFe') is given by

$$\Delta H_{\text{C14vacFe}}^{N-1,M} = \frac{E_{\text{C14vacFe}}^{N-1,M} - (N-1)E_{\text{Fe}} - ME_{\text{Nb}}}{N-1+M}. \quad (5)$$

The formation energy per vacancy

$$E_f^{\text{vac}} = E_{\text{C14vacFe}}^{N-1,M} - E_{\text{C14}}^{N,M} + E_{\text{Fe}} \quad (6)$$

can be rewritten in terms of the structure formation energy (per atom) as

$$\begin{aligned} E_f^{\text{vac}} &= E_{\text{C14vacFe}}^{N-1,M} - (N-1)E_{\text{Fe}} - ME_{\text{Nb}} \\ &\quad - E_{\text{C14}}^{N,M} + (N-1)E_{\text{Fe}} + ME_{\text{Nb}} \\ &\quad + E_{\text{Fe}} \end{aligned} \quad (7)$$

which by comparison to Eqs. 4 and 5 reduces to

$$E_f^{\text{vac}} = (N-1+M)\Delta H_{\text{C14vacFe}}^{N-1,M} - (N+M)\Delta H_{\text{C14}}^{N,M}. \quad (8)$$

With the fraction of the number of defects to the number of atoms in the defect-free supercell of $x_D = 1/(N + M)$ we obtain

$$E_f^{vac} = \frac{(1 - x_D)\Delta H_{C14vacFe}^{N-1,M} - \Delta H_{C14}^{N,M}}{x_D} \quad (9)$$

as formation energy of an Fe vacancy, and correspondingly for a Nb vacancy.

For an antisite defect, e.g. an Fe atom on a Nb site ('C14antiFe'), the formation energy per antisite defect is

$$E_f^{antiFe} = E_{C14antiFe}^{N+1,M-1} - E_{C14}^{N,M} - E_{Fe} + E_{Nb} \quad (10)$$

which can be rewritten as

$$\begin{aligned} E_f^{antiFe} &= E_{C14antiFe}^{N+1,M-1} - (N + 1)E_{Fe} - (M - 1)E_{Nb} \\ &\quad - E_{C14}^{N,M} + (N + 1)E_{Fe} + (M - 1)E_{Nb} \\ &\quad - E_{Fe} + E_{Nb}. \end{aligned} \quad (11)$$

Following the procedure above we obtain

$$E_f^{antiFe} = (N + M)\Delta H_{C14antiFe}^{N+1,M-1} - (N + M)\Delta H_{C14}^{N,M} \quad (12)$$

that reduces to

$$E_f^{antiFe} = \frac{\Delta H_{C14antiFe}^{N+1,M-1} - \Delta H_{C14}^{N,M}}{x_D} \quad (13)$$

and correspondingly for Nb atoms on Fe sites.

Acknowledgements

We acknowledge fruitful discussions with Ali Zendegani and Tilmann Hickel. This work was funded by the German Research Society DFG (project number 289654611).

-
- ¹ A. Sinha, Topologically close-packed structures of transition metal alloys, *Progress in Materials Science* 15 (1972) 81.
 - ² F. Stein, A. Leineweber, Laves phases: a review of their functional and structural applications and an improved fundamental understanding of stability and properties, *Journal of Materials Science* 56 (2021) 5321.
 - ³ B. Seiser, R. Drautz, D. G. Pettifor, TCP phase predictions in Ni-based superalloys: Structure maps revisited, *Acta materialia* 59 (2011) 749.
 - ⁴ B. Seiser, T. Hammerschmidt, A. N. Kolmogorov, R. Drautz, D. G. Pettifor, Theory of structural trends within 4d and 5d transition metals topologically close-packed phases, *Physical Review B* 83 (2011) 224116.
 - ⁵ T. Hammerschmidt, A. Bialon, D. Pettifor, R. Drautz, Topologically close-packed phases in binary transition-metal compounds: matching high-throughput ab initio calculations to an empirical structure map, *New Journal of Physics* 15 (2013) 115016.
 - ⁶ A. Ladines, T. Hammerschmidt, R. Drautz, Structural stability of Fe-based topologically close-packed phases, *Intermetallics* 59 (2015) 59.
 - ⁷ J. D. Livingston, Laves-phase superalloys?, *physica status solidi (a)* 131 (1992) 415.
 - ⁸ M. Heggen, L. Houben, M. Feuerbacher, Plastic deformation mechanism in complex solids, *Nature Materials* 9 (2010) 332–336.
 - ⁹ Y. Zhang, W. Zhang, B. Du, W. Li, L. Sheng, H. Ye, K. Du, Shuffle and glide mechanisms of prismatic dislocations in a hexagonal c14-type laves-phase intermetallic compound, *Phys. Rev. B* 102 (2020) 134117.
 - ¹⁰ K. Kumar, P. Hazzledine, Polytypic transformations in Laves phases, *Intermetallics* 12 (2004) 763.
 - ¹¹ C. W. Allen, P. Delavignette, S. Amelinckx, Electron microscopic studies of the Laves phases TiCr₂ and TiCo₂, *physica status solidi (a)* 9 (1972) 237.
 - ¹² K. Kumar, D. Miracle, Microstructural evolution and mechanical properties of a Cr-Cr₂Hf alloy, *Intermetallics* 2 (1994) 257.
 - ¹³ M. F. Chisholm, S. Kumar, P. Hazzledine, Dislocations in complex materials, *Science* 307 (2005) 701–703.
 - ¹⁴ P. Hazzledine, P. Pirouz, Synchroshear transformations in Laves phases, *Scripta Metallurgica et Materialia* 28 (1993) 1277 – 1282.
 - ¹⁵ W. Zhang, R. Yu, K. Du, Z. Cheng, H. Zhu, J. and Ye, Undulating slip in Laves phase and implications for deformation in brittle materials, *Physical Review Letters* 106 (2011) 165505.
 - ¹⁶ E. Tadmor, S. Hai, A peierls criterion for the onset of deformation twinning at a crack tip, *Journal of the Mechanics and Physics of Solids* 51 (2003) 765.
 - ¹⁷ H. Van Swygenhoven, P. M. Derlet, A. G. Froseth, Stacking fault energies and slip in nanocrystalline metals, *Nature Materials* 3 (2004) 399.
 - ¹⁸ J. Möller, M. Mrovec, I. Bleskov, T. Hammerschmidt, R. Drautz, C. Elsässer, J. Neugebauer, T. Hickel, E. Bitzek, On 110 planar faults in strained bcc metals - origins and implications of a commonly observed artefact of classical potentials, *Physical Review Materials* 2 (2018) 093606.
 - ¹⁹ O. Vedmedenko, F. Rösch, C. Elsässer, First-principles density functional theory study of phase transformations in NbCr₂ and TaCr₂, *Acta Materialia* 56 (2008) 4984 – 4992.
 - ²⁰ L. Ma, T.-W. Fan, B.-Y. Tang, L.-M. Peng, W.-J. Ding, Ab initio study of I2 and T2 stacking faults in C14 Laves phase MgZn₂, *The European Physical Journal B* 86 (2013) 188.
 - ²¹ L. Ma, R.-K. Pan, S.-C. Zhou, T.-P. Luo, D.-H. Wu, T.-W. Fan, B.-Y. Tang, Ab initio study of stacking faults and deformation mechanism in C15 Laves phases Cr₂X (X = Nb, Zr, Hf), *Materials Chemistry and Physics* 143 (2014) 702.
 - ²² S. Voß, M. Palm, F. Stein, D. Raabe, Phase equilibria in the Fe-Nb system, *Journal of Phase Equilibria and Diffusion* 32 (2011) 97–104.
 - ²³ G. Kresse, J. Furthmüller, Efficiency of ab-initio total energy calculations for metals and semiconductors using a

- plane-wave basis set, *Computational Materials Science* 6 (1996) 15.
- ²⁴ G. Kresse, J. Furthmüller, Efficient iterative schemes for ab initio total-energy calculations using a plane-wave basis set, *Physical Review B* 54 (1996) 11169.
- ²⁵ G. Kresse, D. Joubert, From ultrasoft pseudopotentials to the projector augmented-wave method, *Physical Review B* 59 (1999) 1758.
- ²⁶ P. E. Blöchl, Projector augmented-wave method, *Physical Review B* 50 (1994) 17953.
- ²⁷ J. P. Perdew, K. Burke, M. Ernzerhof, Generalized gradient approximation made simple, *Physical Review Letters* 77 (1996) 3865.
- ²⁸ N. Takata, S. Ishikawa, T. Matsuo, M. Takeyama, Transmission electron microscopy of Fe₂Nb Laves phase with C14 structure in Fe-Nb-Ni alloys, *MRS Online Proceedings Library* 1128 (2008) 806.
- ²⁹ M. Slapakova Pokova, S. Voß, K. Kumar, C. Liebscher, F. Stein, Transmission electron microscopy of deformed Laves phase NbFe₂, in: *European Microscopy Congress 2016 Proceedings*, Wiley-VCH, 2016, pp. 263–264.
- ³⁰ J. Guenole, F.-Z. Mouhiba, L. Huber, B. Grabowski, S. Korte-Kerzel, Basal slip in Laves phases: The synchrohear dislocation, *Scripta Materialia* 166 (2019) 134.
- ³¹ D. Thoma, J. Perepezko, A geometric analysis of solubility ranges in Laves phases, *Journal of Alloys and Compounds* 224 (1995) 330.
- ³² C. Liu, J. Zhu, M. Brady, C. McKamey, L. Pike, Physical metallurgy and mechanical properties of transition-metal Laves phase alloys, *Intermetallics* 8 (2000) 1119.
- ³³ A. Ladines, R. Drautz, T. Hammerschmidt, Ab-initio study of C and N point defects in the C14-Fe₂Nb phase, *Journal of Alloys and Compounds* 693 (2017) 1315–1322.
- ³⁴ J. Zhu, L. Pike, C. Liu, P. Liaw, Point defects in binary Laves phase alloys, *Acta Materialia* 47 (7) (1999) 2003 – 2018.
- ³⁵ S. Voß, F. Stein, M. Palm, D. Grüner, G. Kreiner, G. Frommeyer, D. Raabe, Composition dependence of the hardness of Laves phases in the Fe-Nb and Co-Nb systems, *MRS Online Proceedings Library* 1128 (2008) 805.
- ³⁶ N. Takata, H. Ghassemi-Armaki, M. Takeyama, S. Kumar, Nanoindentation study on solid solution softening of Fe-rich Fe₂Nb Laves phase by Ni in Fe-Nb-Ni ternary alloys, *Intermetallics* 70 (2016) 7 – 16.
- ³⁷ F. Chu, D. Pope, Deformation of C15 laves phase alloys, *Materials Research Society Symposium Proceedings* 364 (1994) 1197.
- ³⁸ F. Stein, M. Palm, G. Sauthoff, Structure and stability of Laves phases part II - Structure type variations in binary and ternary systems, *Intermetallics* 13 (2005) 1056.
- ³⁹ M. Slapakova, A. Zendegani, C. Liebscher, T. Hickel, J. Neugebauer, T. Hammerschmidt, A. Ormeci, Y. Grin, G. Dehm, S. Kumar, F. Stein, Atomic scale configuration of planar defects in the Nb-rich C14 Laves phase NbFe₂, *Acta Mater.* 183 (2020) 362–376.